Chapter 3

AuNP/PEDOT-MoS_2 based immunosensor for detection of *Immunoglobulin G (IgG)*

In the previous chapter, an innovative impedimetric detection approach has been discussed utilizing a modified transducer composed of AuNP/GO/PEDOT-PSS. This strategy effectively monitors the changes in interfacial capacitive response relative to antigen concentration affirming the successful adsorption of antigen onto the immunosensor surface. Interestingly, Langmuir adsorption isotherm was observed in case of our immunosensor during the adsorption of analyte. The fabricated sensor offers an effective detection of the specific antigen even at low concentration. Despite the promising capabilities, few limitations such as poor selectivity, moderate LOD and complex experimental procedures were identified. Thus, the primary aim of the current chapter is to address these shortcomings by proposing necessary amendments to the fabrication and detection approaches.

3.1 Introduction

As highlighted in Section 1.4, there is a growing demand for advancing sensor technology for accurate determination of various biomarkers at clinical level diagnosis. In case of electrochemical sensor, the transducer plays a crucial role in overall performance of the sensor. In Chapter 2, we have designed AuNP/GO/PEDOT-PSS based immunosensor for impedimetric determination of the specific antigen. Besides, low sensitivity and poor selectivity are two major drawbacks associated with this system. This can be further improved by modifying the transducer and following alternate detection approaches. The impedimetric detection method of earlier work suffers from poor signal amplification causing fluctuation in the capacitive response as can be seen in Figure 2.11. This is attributed to the minute change in capacitance value that is influenced by the surrounding causing disturbances in signal. In this regard, amperometry detection can deliver better signal amplification with high precision. On the other hand, PEDOT-PSS offers a low conductivity value due to the presence of insulating PSS counterpart. Similarly,

conductivity of GO is very low due to the abundance of oxidative groups on its surface. So, replacing PEDOT-PSS and GO with PEDOT and 2D layered MoS_2 is expected to be a useful strategy for enhancing the interfacial electron transport mechanism. Currently, MoS_2 is considered to be an emerging candidate for enhancing the physicochemical properties of the CP based electrocatalyst [167]. MoS_2 is being explored extensively in the domain of electrochemical sensing due to its graphene like structure with tunable band gap. Also, larger interlayer spacing, higher carrier mobility, hydrophilic nature and faster in plane charge transfer are some of the advantages offered by this layered inorganic material which opens some novel approaches in the field of sensing [168]. Moreover, as mentioned in earlier chapter, a thin layer of AuNPs will be beneficial for improving the electrochemical activity resulting a better sensor performance.

In this work, we have designed an immunosensor probe by electrodepositing AuNPs on the surface of PEDOT-MoS_2 composite system followed by immobilizing mouse *IgG* antibody over the modified electrode system *via* glutaraldehyde cross-linking method. The amperometric detection of the specific analyte (goat anti-mouse *IgG*) using our prepared immunosensor will be carried out in PBS solution containing 5 mM ferrocyanide as a redox agent. Using a redox probe, it can sufficiently amplify the amperometric signal of the redox peaks. The fabrication technique and sensing mechanism of our proposed sensor has been portrayed in Figure 3.1. The change in the peak current in differential pulse voltammetry (DPV) response after antibody-analyte interaction stipulates the presence and concentration of the specific analyte in the electrolytic solution.

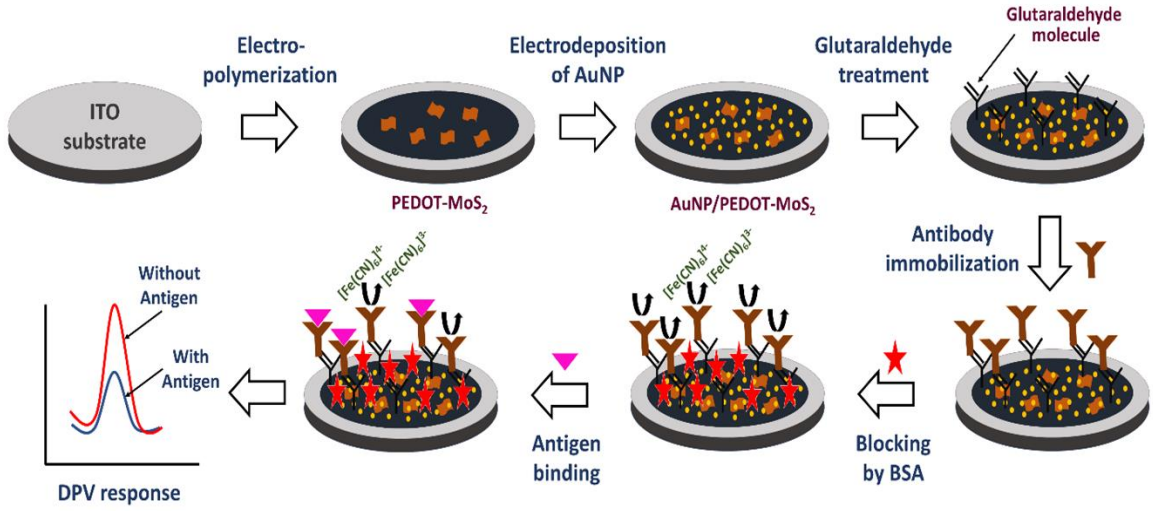

Figure 3.1: Schematic illustration of the immunosensor fabrication and detection mechanism

3.2. Experimental

3.2.1. Synthesis of PEDOT/ITO electrode

The PEDOT film was first electrodeposited over the ITO substrate by chrono-amperometric technique. The experimental setup is already described in section 2.2.1 of Chapter 2. Firstly, an electrolyte solution was prepared in acetonitrile containing 0.1 M EDOT along with 0.05 M $LiClO_4$. In previous work, the synthesis of polymer film was performed via CV technique which consumes more time for completion of multiple cycles to complete. In Figure 2.1 (a), one can see that the anodic current in the CV cycles is very high beyond +1.0 V indicating efficient polymerization of EDOT monomer beyond that potential value. That's why, a fixed dc potential of +1.1 V was applied in the chronoamperometry experiment for deposition of PEDOT over ITO substrate. A blackish-blue thick film has appeared after running the chronoamperometry for 80 s. This confirms the electro-polymerization of EDOT units to PEDOT polymer system.

3.2.2. Hydrothermal processing of layered MoS_2

MoS_2 nanostructure was prepared by using ammonium molybdate and thiourea as precursors. 1 M aqueous solution of ammonium molybdate and 4 M thiourea solution were prepared separately in 30 mL beakers. Then transferred them into a teflon-lined stainless-steel autoclave (100 mL) and the hydrothermal reaction was carried out at a temperature of 200^0 C, for 24 h. The autoclave was cooled naturally to room temperature. Finally, the black precipitate was collected and washed with DI water and AR-grade ethanol followed by drying overnight at a temperature of 80^0C [169].

3.2.3. Synthesis of PEDOT-MoS_2/ITO electrode

Similar experimental setup was used as mentioned in section 3.2.1 for synthesis of PEDOT-MoS_2 deposited ITO electrode. For this, 0.1 M EDOT is prepared in 15 mL acetonitrile solution containing 350 μL of 1 mg/mL aquous MoS_2 suspension. 0.05 M $LiClO_4$ is added in the solution followed by sonication for 20 minutes. Then chronoamperometry has been run at an applied oxidation potential of +1.1 V for 80 seconds. Appearance of dark blue coloured film over the ITO substrate indicates the electro-polymerization of EDOT monomer by entrapping layered MoS_2 sheets in and over the polymer matrix to form the PEDOT-MoS_2 composite.

3.2.4. Synthesis of AuNP/PEDOT-MoS_2/ITO electrode

The deposition procedure of AuNPs over PEDOT-MoS_2 system is same as discussed in section 2.2.4 of Chapter 2. Here, we used already synthesized PEDOT-MoS_2/ITO as

working electrode in the experimental setup and ran the CV for 5 cycles at 20 mV/s scan rate under potential window of -0.2 V to +1.1 V. Afterwards, the AuNP deposited composite system was stored in a desiccator for further use.

3.2.5 Fabrication of the immunosensor

Glutaraldehyde cross-linking method has been followed to immobilize the mouse *IgG* antibody over the prepared electrode systems, as described in section 2.2.5. The cross-linking agent, glutaraldehyde can attach with the functional moieties and polar segments of the composite polymer system offering adequate immobilization of the antibody. Finally, the fabricated immunosensor was stored at a temperature of 4^{o}C until further use.

3.3. Results and discussion

3.3.1. X-ray diffraction and infrared spectroscopy analyses

In this work, we followed the similar sample preparation procedure as explained in section 2.3.1. The XRD patterns of PEDOT, PEDOT-MoS_2 and AuNP/PEDOT-MoS_2 deposited ITO electrodes are depicted in Figure 3.2 (a). Being an amorphous system, PEDOT doesn't exhibit any sharp diffraction peak in the XRD pattern. Whereas, the prominent peaks appearing in response (i) of Figure 3.2 (a) are due to the ITO substrate over which PEDOT is electro polymerized. The hump appearing around, 2θ ~25^o indicates the semi-crystalline nature of PEDOT system. Other sharp peaks appearing in this response are due to the presence of ITO at the base of the film, as mentioned in section 2.2.1 of Chapter 2. In response (ii), the sharp diffraction peak observed at 2θ =14.5^o corresponds to the (002) plane of the MoS_2 [170]. Appearance of both MoS_2 characteristic peak and the polymer hump in this response indicates the presence of TMDC and polymer components in the composite system. In the pattern (iii) of Figure 3.2 (a), the characteristic peak of Au appeared at 2θ=38.6^o, that resembles (111) diffraction plane of the electrodeposited Au nanoparticles having average crystallite size of 20.98 nm (estimated from Scherrer's formula described in section 1.5.1). Other peaks appearing at 2θ = 44.7^o, 65.0^o and 77.9^o corresponded to the (002), (022) and (113) planes of the face centered cubic (*fcc*) Au crystals (ICDD ref No. 00-004-0784), respectively. The Au diffraction peaks appeared to be highly intense in response (iii) due to the presence of AuNP at the surface of PEDOT-MoS_2 composite system. The intense peaks of Au have dominated the diffraction hump of PEDOT and suppressed the MoS_2 characteristic peak in the AuNP/PEDOT-MoS_2/ITO hybrid system.

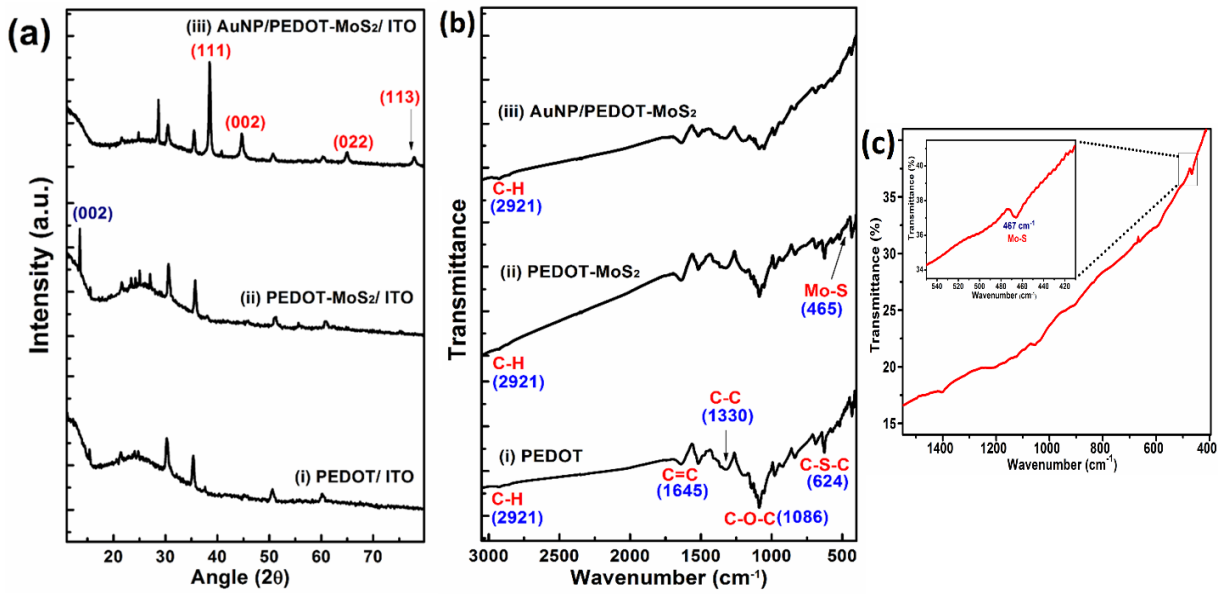

Figure 3.2: (a) XRD pattern, and (b) FT-IR response; of PEDOT, PEDOT-MoS_2 and AuNP/PEDOT-MoS_2 systems. The zoomed in view of FT-IR response of MoS_2 is shown in Figure (c)

The sample preparation for FT-IR study was similar as outlined in section 2.3.2. The IR response of the system electrodes have been represented collectively and compared accordingly as shown in Figure 3.2 (b). In spectrum-(i), the vibrational band appeared at ~ 624 cm^{-1} and 1645 cm^{-1} which are due to the C-S-C bond vibration and symmetric C=C stretching of the thiophene ring. Vibrational modes obtained around 1086 cm^{-1} and 1330 cm^{-1} corresponded to the symmetric C-O-C stretching and C-C bond vibration of PEDOT respectively. Another vibrational band around 2921 cm^{-1} signifies C-H bond stretching, which is very less significant in response-(i) but becomes substantial in PEDOT-MoS_2 and AuNP/PEDOT-MoS_2 systems as can be viewed in the Figure. The IR spectra of synthesized MoS_2 are provided in the Figure 3.2 (c). In case of MoS_2, we have obtained a smooth spectrum declining sharply towards the higher wavenumber region with Mo-S vibrational mode ~ 466 cm^{-1} (can be viewed clearly in the magnified image). The FT-IR response of PEDOT-MoS_2 system is depicted in spectrum-(ii) of Figure 3.2 (b), that exhibits similar vibrational modes like PEDOT with reduced intensity. Moreover, the Mo-S vibrational band has been suppressed in the composite system that appears at, ~ 466 cm^{-1} [171]. After incorporation of MoS_2 in the polymer system, the freely suspending polymer chains are constrained by the corrugated MoS_2 nanosheets, resulting in a decrease in vibrational band intensity in the IR spectrum as in (ii) of Figure 3.2 (b). In addition, the sharp declining of

the IR response towards higher wavenumber region can be seen in the PEDOT-MoS_2 composite system which was earlier observed in MoS_2. In the third spectrum *i.e.*, AuNP/PEDOT-MoS_2 system, we can see some suppression of the vibrational bands followed by disappearance of the modes, which may be due to the deposition of AuNPs over the composite matrix that has probably been generating constraints against stretching of the molecular bonds.

3.3.2. FE-SEM and energy dispersive X- ray analyses

The respective FESEM micrographs of PEDOT, PEDOT-MoS_2 and AuNP/PEDOT-MoS_2 were captured as shown in Figure 3.3(a)-(c). The associated EDX spectra depict the elemental constituents of each of the systems. The distribution of the PEDOT grains all over the ITO substrate can be seen in Figure 3.3(a) where the polymer units, seemed to be mutually connected with each other. During electro-polymerization, the EDOT monomer lose one electron to the working electrode and forms cationic radical. The charge instability in the cationic radical strips away the H^+ from the sp^2 hybridized C-atom which is located next to the sulfur atom of the sulfonic ring. This electron rich C-atom then covalently binds with the nearby cationic radicals by sharing its unpaired electron and subsequently forms long polymer chain. Such nanostructures can provide high surface area, superior electrolytic contact and good electron conduction mechanism driven by carrier hopping. The entrapment of the MoS_2 sheets in the PEDOT matrix can be realized from Figure 3.3(b). Prior to EDOT polymerization in MoS_2 dispersed solution, some of the EDOT $^{0+}$ cationic radicals can get attached over the MoS_2 sheets present in the electrolyte solution. Upon electro-polymerization, these MoS_2-surface attached monomers were polymerized over the conducting ITO surface by holding the MoS_2 sheets in between the polymer matrix. This can be viewed in the FESEM image of PEDOT-MoS_2 system where the MoS_2 sheets are distributed like bunches of flower petals in the PEDOT system. This flower like morphology usually provides maximum surface area to the system for better interfacial contact [172]. Again, Figure 3.3(c) depicts the flower petal like MoS_2 sheets surrounded by polymer units. Upon close observation, one can notice that surface roughness of the third system is higher as compared to the PEDOT-MoS_2 one, indicating the growth of spherical AuNPs over the polymer grains. After few layers of deposition, this surface anchored AuNPs have made the surface of the PEDOT-MoS_2 film rough and uneven. In addition, the presence of Au in this system can be confirmed from the absorption peak of Au appearing at ~ 2.2 keV in the EDX spectrum of Figure 3.3(c). However, the inner shell X- ray

absorption spectra of C, O, S, Mo and Au in the EDX responses of Figure 3.3(a)-(c) have substantiated the formation of the composite system at large. The atomic percentage of the elemental constituents corresponding to all the three systems are shown in the inset tables.

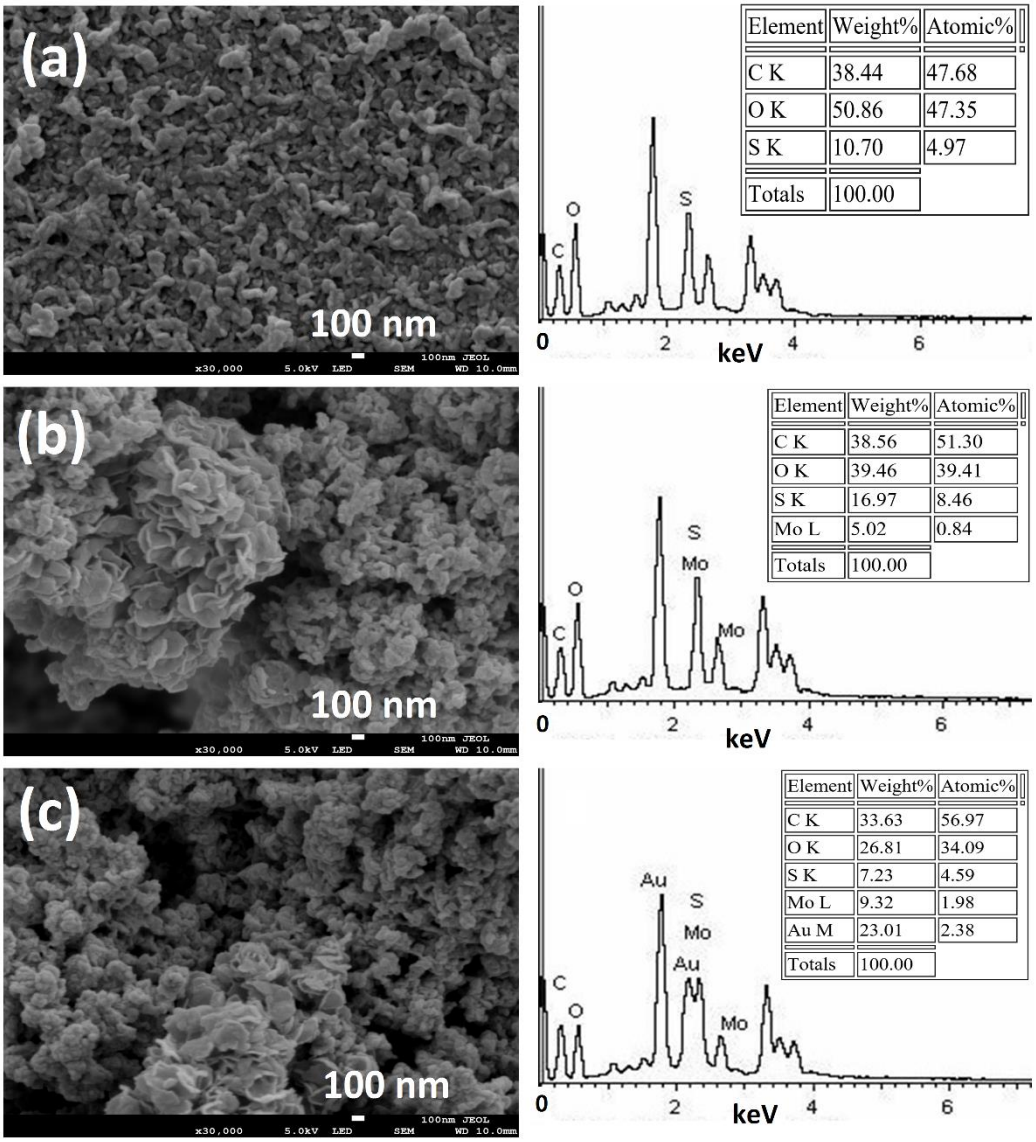

Figure 3.3: FESEM micrograph and EDX spectra of (a) PEDOT, (b) PEDOT-MoS_2 and (c) AuNP/ PEDOT-MoS_2

3.3.3 Comparative cyclic voltammetry (CV) studies of as-fabricated electrodes

The experimental setup for performing CV is the same as described in section 2.3.5 of Chapter 2. The previous work demonstrates the detection of the specific antigen by impedometric technique. But during this work, we have followed an amperometric detection protocol. In general, PBS electrolyte is neutral (pH=7.4) in nature and offer poor

amperometric response due to the absence of active redox agent. To address this limitation, electrochemical measurements throughout this study are conducted using a 10x PBS solution containing 5 mM $K_3[Fe(CN)_6]$ as redox probe.

At first, the PEDOT/ITO, PEDOT-MoS_2/ITO and AuNP/PEDOT-MoS_2/ITO electrodes are subjected to assessment through the CV features under a potential range of -0.4 V to +0.2 V and at a scan rate of 20 mV/s. Here, the initial (V_i) and final (V_f) voltages of the CV cycles are assigned at 0 V w.r.t. the reference electrode (R.E.). In the beginning of the voltametric scan (V_i = 0 V), no diffusion layer has been generated over the W.E. But during the cathodic potential sweep, the reduction of, $[Fe(CN)_6]^{3-} + e^- \rightarrow [Fe(CN)_6]^{4-}$ occurs along with the formation of diffusion layer over the W.E. As the potential becomes more negative, the thickness of the diffusion layer increases which hinders the mass transport of $[Fe(CN)_6]^{3-}$ radical towards the electrode. This results in a declining trend of the reduction current in the CV cycle. To be mentioned, the limiting potential in the CV response after which the reduction current started to decline due to the inefficient mass transport of the $[Fe(CN)_6]^{3-}$ radical towards the W.E. is termed as reduction peak potential (E_{pc}). Afterwards, the scanning direction of voltage is reversed at the switching potential of -0.4 V and oxidation peak has been obtained in between -0.2 V to 0 V potential range during the anodic scan. The scanning potential is again reversed at +0.2 V and then it sweeps down to the final voltage of 0 V. Though the CV cycles had started and ended up at the same potential, the concentration gradient formed over the W.E. are different for both the temporal events. Therefore, we have obtained dissimilar current values at the 0 V potential position for both initial and final voltages of the scan, which results in the breaking of the current response at 0 V of the CV cycle. In Figure 3.4 (a), the height of the oxidation (I_{pa}) and reduction peak current (I_{pc}) for PEDOT/ITO system are found to be at 141.5 µA and -177.7 µA; respectively. However, after incorporation of MoS_2 and AuNP layer, the values of I_{pa} and I_{pc} tending to augment up to 268.5 µA (oxidation) and -346.6 µA (reduction); respectively. This would indicate a significant improvement in the electrocatalytic activity of the modified system towards $[Fe(CN)_6]^{3-/4-}$ redox process. Moreover, the anodic (E_{pa}) and cathodic (E_{pc}) peak potential separation for PEDOT, PEDOT-MoS_2 and AuNP/PEDOT-MoS_2 systems are 161 mV, 84 mV and 59 mV, respectively. The decrease in peak separation (ΔE_p) value suggests that higher number of electrons transfer (n) is taking place throughout the redox process of the modified system (as, $n \propto 1/\Delta E_p$) [173]. In the CV responses of Figure 3.4 (a), the ratio of the peak currents (I_{pa}/I_{pc}) ~ 0.97 and ΔE_p

value decreases to 59 mV upon insertion of MoS_2 and AuNP. It indicates that after modification, the system is tending towards reversibility with a superior reaction kinetics as compared to the pristine one. But as the scan rate (v) is varied from 20-100 mV/s, the value of ΔE_p increases noticeably as can be seen in Figure 3.5 (a-c)), suggesting that the redox process taking place in the electrode systems are not completely reversible and it moderately depends upon the rate constant (k_s) of the electrochemical reaction [174]. Moreover, a linear variation of peak current (I_p) *vs.* square root of scan rate ($\sqrt{v}$) plots shown in Figure 3.5 (a.1-c.1) featuring a diffusion-controlled redox process in case of all the three distinct electrode systems, prior to bioconjugation [175].

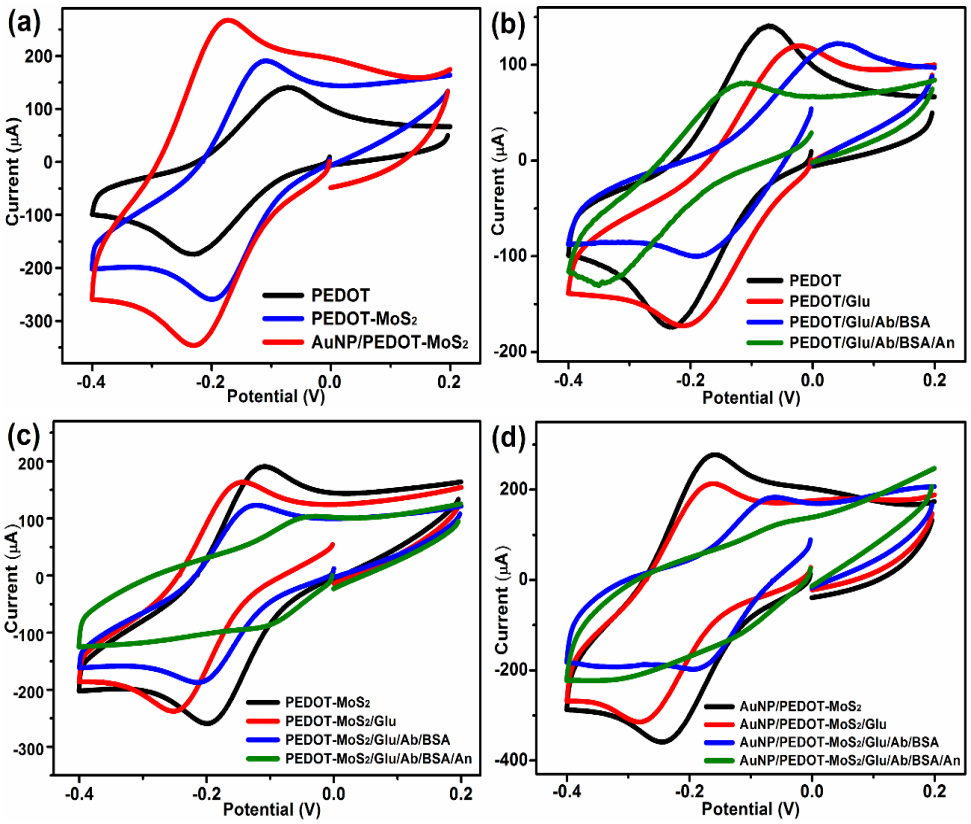

Figure 3.4: CV response of (a) PEDOT, PEDOT-MoS_2 and AuNP/ PEDOT-MoS_2 electrodes, and that of (b) PEDOT, (c) PEDOT-MoS_2 and (d) AuNP/ PEDOT-MoS_2 sensor electrodes at different process steps throughout the sensing experiment.

The electroactive area of the as prepared electrode for the non-reversible process can be determined by using the modified Randle-Sevcik equation that gives a direct linear relation between the I_p *vs.* $\sqrt{\nu}$ stated as [176],

$$I_p = 2.99 \times 10^5 \times n^{3/2}\alpha^{1/2}AD^{1/2}C\nu^{1/2} \text{ , (at T= 300 K).} \quad (3.1)$$

Here, n (=1) is no. of electron transfer taking place in the redox process, D is diffusion coefficient, A is electroactive area, α is transfer coefficient of the redox process and C (=5 mM) is the concentration of K_3 [Fe $(CN)_6$] in the PBS solution. The molecular diffusion coefficient in water is typically in the order of 10^{-5} cm^2/s [**177**]. So, we have considered D ~ 10^{-5} cm^2/s. The value of A can be determined from the slope (ζ) of the I_p *vs.* $\sqrt{\nu}$ plot as, $A = \frac{\varsigma}{2.99\times10^5\times n^{3/2}C\alpha^{1/2}D^{1/2}}$. From the slope of the linear region of E_{pa} vs $log(\upsilon)$ plot (Figure 3.5 (a.2-c.2)), the respective values of α for PEDOT, PEDOT-MoS_2 and AuNP/PEDOT-MoS_2 electrodes have been calculated as 0.39, 0.42 and 0.37. For a diffusion controlled ($I_p \propto \upsilon^{1/2}$) process, the anodic peak potential (E_{pa}) depends linearly on $log(\upsilon)$ as [178],

$$E_{pa} = \frac{2.3RT}{2\alpha nF} log\upsilon + constant. \quad (3.2)$$

Here, R is the universal gas constant (= 8.3145 J $mol^{-1}K^{-1}$), T is absolute temperature and F is Faraday's constant (= 96,485 Coulomb/mol). In Figure 3.5 (a.2-c.2), only the anodic peak potential (E_{pa}) has been plotted w.r.t. the *log* (scan rate), as we have considered the oxidation scan of the differential pulse voltammetry (DPV) response while sensing. Accordingly, the electroactive areas (for oxidation of the redox couple) associated with the PEDOT, PEDOT-MoS_2 and AuNP/PEDOT-MoS_2 systems were estimated to be 11.5×10^{-4}, 16.5×10^{-4} and 21.0×10^{-4} cm^2; respectively. This marginal increase in the electroactive area indicates that the redox activity as well as kinetics of the redox process have been enhanced synergistically after incorporation of MoS_2 and AuNPs in the polymer system.

In Figure 3.4 (b), (c) and (d), the CV responses of PEDOT, PEDOT-MoS_2 and AuNP/PEDOT-MoS_2 electrodes were shown after considering different process steps *viz.* glutaraldehyde addition, antibody (mouse *IgG*) immobilization and antigen (goat anti-mouse *IgG*) interaction. Apparently, the peak heights (I_p) tend to fall, while peak separation (ΔE_p) gets enhanced in all the systems under study after enduring each step. This is because, after addition of glutaraldehyde which is a reactive di-aldehydic group gets attached/absorbed over the electrode surface by blocking the active redox sites resulting in a decrease in peak current values. After that, upon addition of 100 µg/mL of mouse *IgG* antibody, they covalently bind/immobilized over the glutaraldehyde treated film. This

results in further blocking of the active sites that ended up lowering the electron transfer in between electrode-electrolyte interface which can also be confirmed from the increase in the ΔE_p values of the CV cycles taken after immobilization of the antibody. Basically, the fabrication of immunosensor involves immobilization of the antibody over the substrate electrode, which usually leads to the degradation of redox activity and increase in contact resistance of the base substrate or transducer. So, we took help of some classical methods to understand the electrochemical behaviour of the fabricated immunosensor.

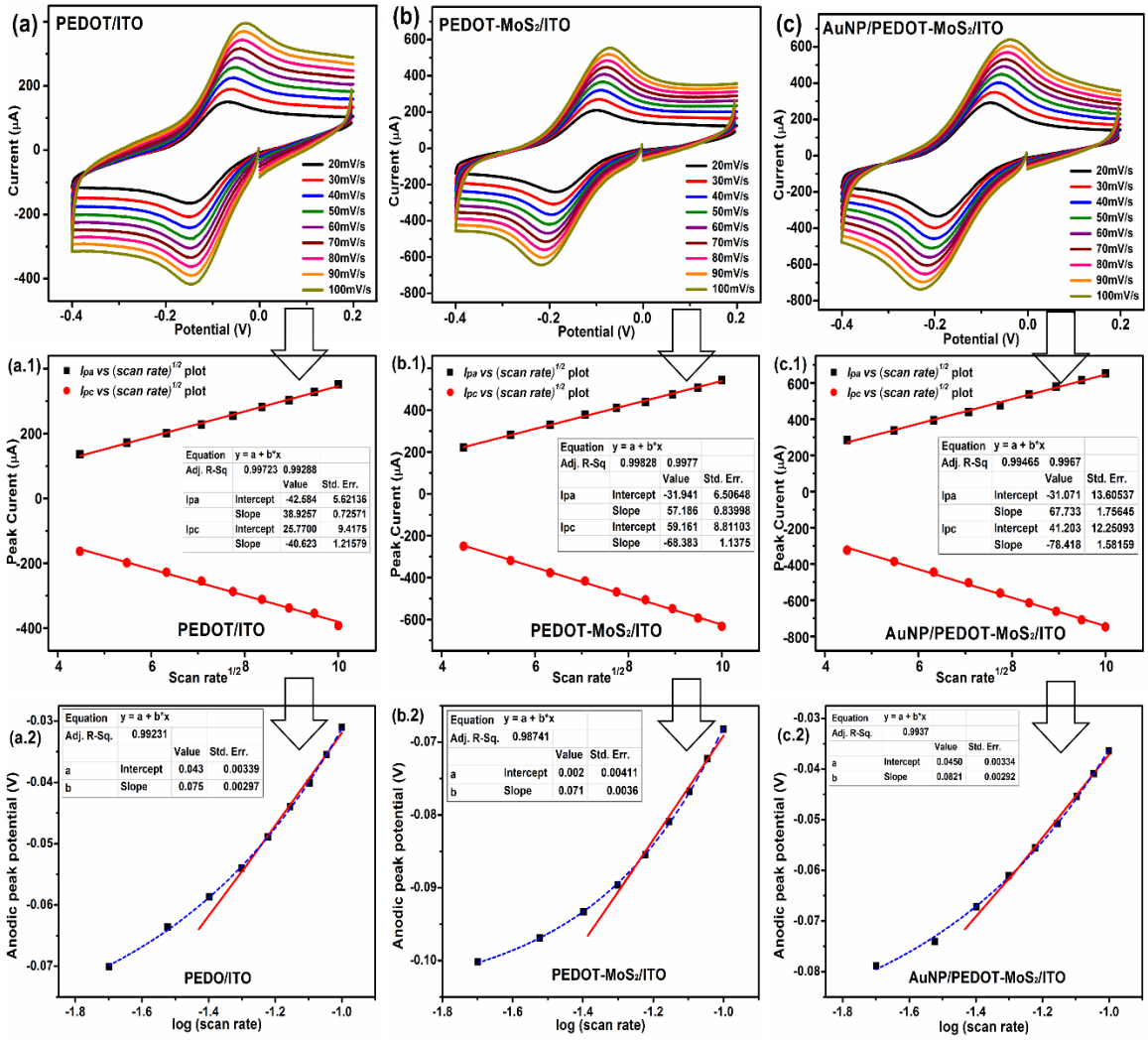

Figure 3.5: Cyclic voltammetry responses taken by varying scan rate for (a) PEDOT, (b) PEDOT-MoS_2 and (c) AuNP/PEDOT-MoS_2 electrodes. Peak potential (v) vs root of scan rate ($v^{1/2}$) plot of the CV responses of (a.1) PEDOT, (b.1) PEDOT-MoS_2 and (c.1) AuNP/PEDOT-MoS_2. Anodic peak potential (E_{pa}) *vs* log (scan rate) plot of (a.2) PEDOT, (b.2) PEDOT-MoS_2 and (c.2) AuNP/PEDOT-MoS_2 electrode systems

Prior to sensing, we have estimated the electroactive area (A) of the as-fabricated BSA/Antibody/Glu/AuNP/PEDOT-MoS_2 immunosensor by using the previously discussed method and thus from Figure 3.6 (a-c) the value of A has been found as, A=9.8x10^{-4} cm^2. Here, the electroactive area has been reduced to almost half after immobilization of the antibody over the composite substrate electrode. Antibody being a complex macromolecule, sits over the substrate electrode by blocking its redox active sites which makes the transducer less accessible for redox agents as well as hinders the smooth mass transport towards the electrode. This gives rise to poor interfacial charge transfer and sluggish kinetics of the redox process after antibody immobilization.

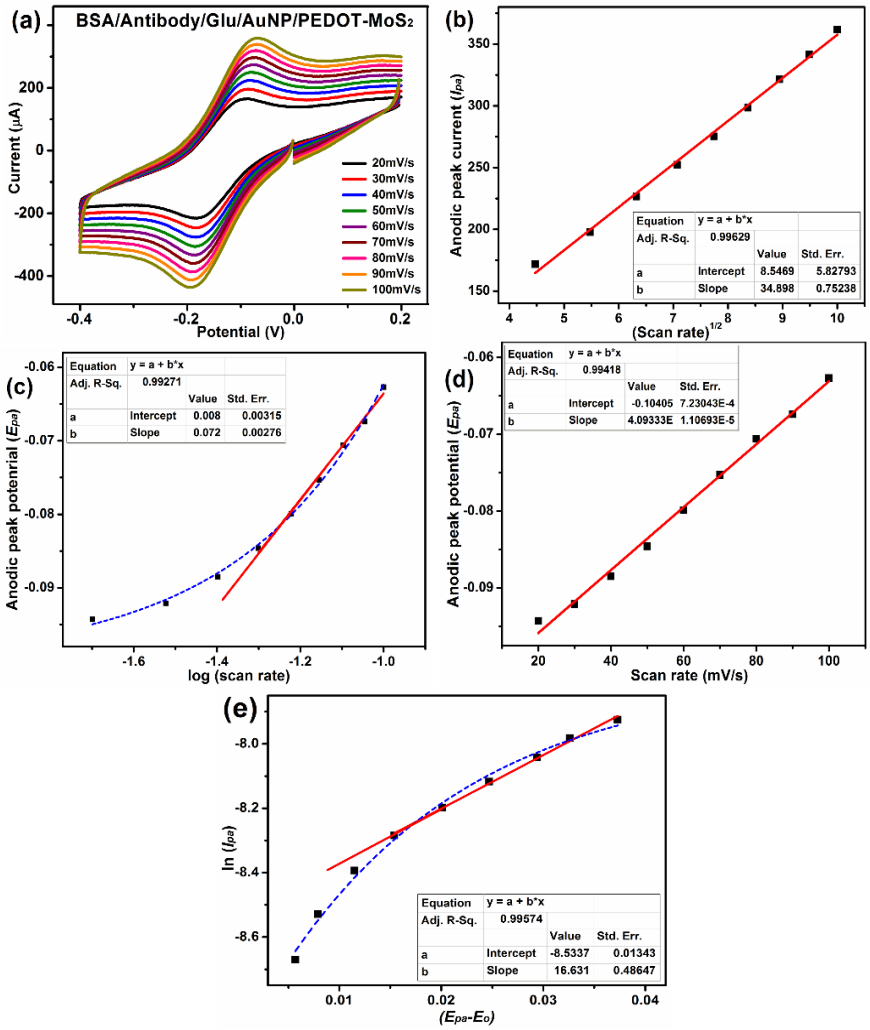

Figure 3.6: (a) Scan rate variation plot, (b) anodic peak current (I_{pa}) vs (scan rate)$^{1/2}$ plot, (c) anodic peak potential (E_{pa}) vs log (scan rate) plot, (d) E_{pa} vs log (scan rate) plot, (e) log_e (I_{pa}) vs (E_{pa}-E_o) plot; for BSA/Antibody/Glu/ AuNP/PEDOT-MoS_2 bioelectrodes.

To study the kinetics, we have calculated the rate constant (k_s) of the BSA/Antibody/Glu/AuNP/PEDOT-MoS_2 immunosensor system towards the redox process of $[Fe(CN)_6]^{3-/4-}$. For a non-reversible redox process, the peak current (I_p) depends upon the reaction rate (k_s) as [179],

$$I_p = 0.227FAk_sC.\exp\{\frac{-\alpha F}{RT}(E_p - E_o)\}$$

$$\text{or} \qquad ln(I_p) = ln(0.227FAk_sC) - \frac{\alpha F}{RT}(E_p - E_o) \qquad (3.3)$$

Here, E_o and E_p denotes the formal electrode potential and redox peak potential, respectively. Going through the plots of Figure 3.6(d, e) and using above relations, the value of α and k_s are estimated to be 0.42 and 0.0019 s^{-1}. It is worth noting that, the value of k_s that lies in between 0.02 to 5×10^{-5} would signify the quasi-reversible behaviour of the system [180]. Lastly, after addition of antigen in the solution, the antibody-antigen locking would take place and a thick interlayer is formed at the interface that hinders the diffusion of charge towards the sensor electrode. As a result, suppression/disappearance of the redox peak can be observed in the CV data acquired after interacting with antigen molecules. From the above observations, one could adjudge effective immobilization of the antibody over the fabricated sensor electrodes via glutaraldehyde cross-linking and antibody-antigen locking interactions. During the fabrication and sensing steps, the substrate electrodes experienced suppression, dislocation, and disappearance of the redox peaks in the CV curves which have been captured at different steps throughout the experiment.

3.3.4. Electrochemical impedance studies of the sensor electrodes

The EIS responses of the electrode systems are captured over a frequency range of 1 Hz to 1 MHz with no applied bias potential. The experimental setup described in section 3.3.3 has been used for acquiring the EIS spectra. The impedance spectra of PEDOT, PEDOT-MoS_2 and AuNP/PEDOT-MoS_2 electrodes are plotted and shown in Figure 3.7 (a). The respective fitted parameters are enlisted in Table 3.1. Here, the solid lines signifying the experimentally obtained impedance data while the dotted lines representing fitted spectra. The inset diagram in Figure 3.7 (a) is the equivalent Randle circuit which is employed to fit all the impedance spectra (besides, a different Randle circuit has been used for fitting the EIS spectra of Antigen/BSA/Antibody/Glu/AuNP/PEDOT-MoS_2 in Figure 3.7(d)). The equivalent circuits are considered after examining the behaviour of the Nyquist plots. In the obtained plot, the appearance of small semicircle in high frequency region indicates the presence of parallelly aligned capacitive and resistive interfaces. Also, the appearance of

long tail in low frequency region hints towards the diffusive nature of the electrode system due to the formation of complex interfaces in the hybrid electrode as well as in the biomolecules immobilized systems. In the equivalent circuit, all the parameters have their usual meanings as outlined in section 2.3.6 of Chapter 2. A noticeable declining of the R_{ct} value from 75.64 Ω to 24.8 Ω would indicate a better interfacial charge transfer event taking place upon AuNP surface deposit as well as incorporation of layered MoS_2 in the PEDOT host (Table 3.1).

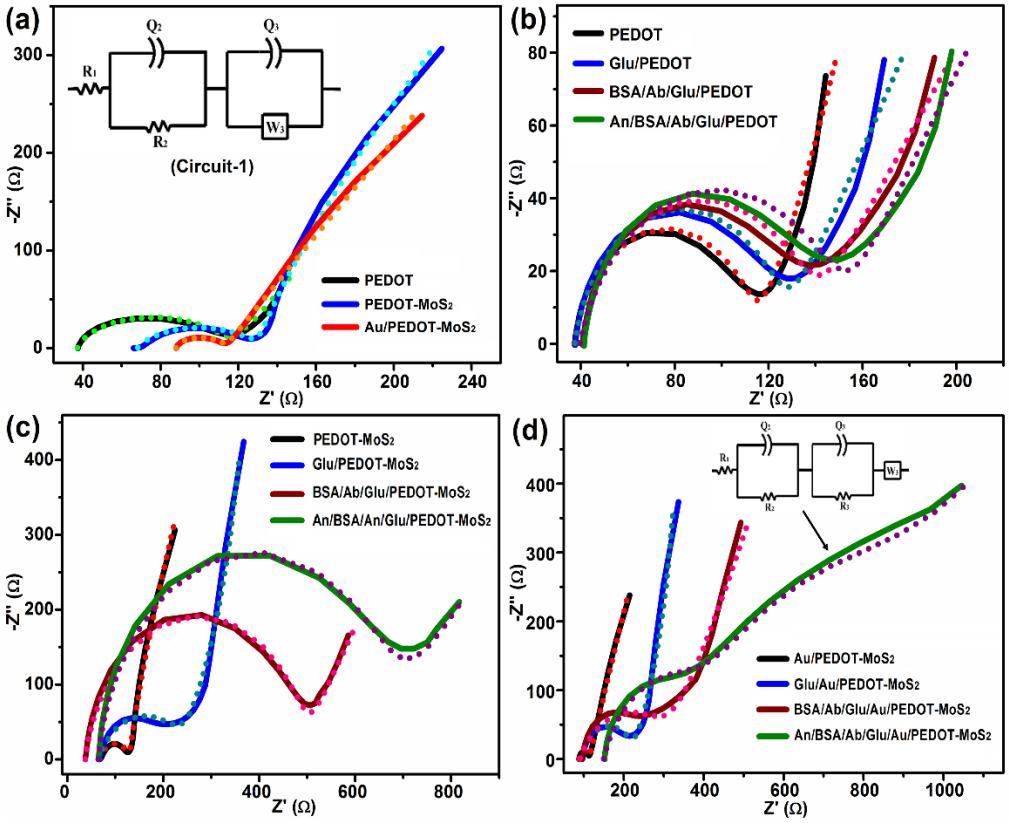

Figure 3.7: EIS responses of (a) PEDOT, PEDOT-MoS_2 and AuNP/PEDOT-MoS_2 electrodes, (b) PEDOT, (c) PEDOT-MoS_2 and (d) AuNP/PEDOT-MoS_2 sensor electrodes at different process steps throughout the sensing experiment.

Also, an overall ten-fold decrease in C_{dl} value can be seen in the composite system, offering values in the range 19.9 to 1.8 mF which accounts for an enhancement in the faradic charge transfer process. The additional MoS_2 and AuNPs act as an intermediate shuttle in the electron hopping mechanism of the polymer matrix, which resulted a decrease in R_{ct} value and increase in faradic charge transfer. However, the Q_3 value gets enhanced after insertion of MoS_2 into the PEDOT polymer but falls upon deposition of AuNP surface layer, possibly due to the shrinking of the interfacial gaps in between PEDOT grains and

MoS_2 sheets that are occupied by electrodeposited metal NPs. To be mentioned, the PEDOT largely exhibit capacitive behavior at a lower frequency region. On the other hand, the composite systems impart diffusive nature at lower frequencies which can be realized from the long-inclined tail of the impedance spectra in Figure 3.7(a). Moreover, the Warburg impedance value obtained also confirms the diffusive nature of the PEDOT-MoS_2 and AuNP/PEDOT-MoS_2 composite systems (Table 3.1). The diffusive mass transport of ions and radicals is driven by the concentration gradient and potential gradient generated in the electrolytic solution along with the porous structure of the sensor probe.

Table 3.1: Fitted EIS parameters of the electrode systems.

Electrode-type	R_1 **(Ω)**	R_2 **(Ω)**	Q_2 **($\times 10^{-3}$ F)** η	Q_3 **($\times 10^{-6}$ F)** η	W_3 **($S.s^{1/2}$)**
PEDOT	37.12	75.64	19.91 η= 0.546	8.817 η= 0.868	17.32×10^{-3}
PEDOT-MoS_2	68.08	62.21	1.008 η= 0.928	20.63 η= 0.750	0.5364×10^{-3}
AuNP/PEDOT-MoS_2	87.99	24.80	1.879 η= 0.755	6.878 η= 0.894	0.00308×10^{-3}

The EIS spectra plotted for PEDOT, PEDOT-MoS_2 and AuNP/PEDOT-MoS_2 nano systems through different stages of the experiment can be found from Figure 3.7 (b-c). The R_{ct} value tends to increase after glutaraldehyde treatment and antibody immobilization followed by blocking of active sites using BSA. This may be because, after each process steps, an additional layer is formed over the film that could increase the width of the electric double layer (EDL) in between electrode-electrolyte interface and thus contributing to higher value of charge transfer resistance. Moreover, upon addition of antigen (goat-antimouse *IgG*) in the solution, it binds with the biorecognition element (mouse *IgG*) creating antibody-antigen (*Ab-An*) pairs. These *Ab-An* pairs further augment the thickness of the double layer by forming new dielectric coatings over the sensor that hinders the charge transport at the interface. Therefore, after addition of antigen in the PBS solution, the R_{ct} value increases substantially for all the three systems. The hindrance in charge transfer events can also be realized in the characteristic CV responses where suppression and disappearance of redox peaks occurred after adding antigenic serum in the solution (Figure 3.4).

To understand the interfacial charge transport and interlayer mechanism, the fitted parameters associated with the AuNP/PEDOT-MoS_2 system were analyzed at various phases of the sensor development procedure as can be found from Table 3.2. The R_{ct} value increases from 24.8 Ω to 410 Ω during the different stages of the experiment *viz*. glutaraldehyde cross linking, antibody immobilization and antibody-antigen interaction. Also, an increase in Q_2 and Q_3 values throughout each experimental steps (upto antibody immobilization) indicating an increase in the capacitive behavior due to the widening of the EDL. But after *Ab-An* interaction, the charge transport has become more complex. As two semi-circles have been developed in the Nyquist plot in case of Antigen/BSA/ Antibody/Glu/AuNP/PEDOT-MoS_2 system **(**Figure 3.7(d)). The dielectric layer of *Ab-An* abduct features the formation of additional solid-electrolyte interphase (SEI) layer over the electrode interface that results in the appearance of the small semicircle at the high frequency region in this Nyquist plot [21]. The equivalent Randle circuit is inserted in this Figure that delivers a generous fit for the EIS spectra of Antigen/BSA/ Antibody/Glu/AuNP/PEDOT-MoS_2 electrode system. Here, the additional term R_3 (=222.3 Ω) is the resistance offered by the additional SEI layer. The formation of two electrochemically distinguishable SEI layers have actually influenced the Q_2 and Q_3 values, as the regular variation of CPE (Q) values is tending to alter in the present scheme.

Table 3.2: Fitted EIS parameters for AuNP/PEDOT-MoS_2 sensor electrode during different steps of the sensing experiment.

Sensor electrode	R_1 **(Ω)**	R_2 **(Ω)**	Q_2 **($\times 10^{-3}$ F)** η	Q_3 **($\times 10^{-3}$ F)** η	W_3 **($S.s^{1/2}$)**	
AuNP/PEDOT-MoS_2	87.99	24.80	1.879 η= 0.755	6.878 η=0.894	3.080×10^{-5}	
Glu/AuNP/PEDOT-MoS_2	97.87	121.6	17.55 η= 0.528	14.34 η= 0.816	16.53×10^{-3}	
BSA/Antibody/Glu/AuNP/ PEDOT-MoS_2	89.98	211.6	10.19 η= 0.522	49.89 η= 0.648	8.848×10^{-3}	
Antigen/BSA/Antibody/Glu /AuNP/PEDOT-MoS_2	149.20	410.03	0.273 η= 0.765	19.01 η= 0.803	R_3 **(Ω)**	W_3 **($S.s^{1/2}$)**
					222.3	1.348×10^{-3}

3.3.5. Detection of specific antigen and estimation of analytical parameters

The response of the mouse *IgG* immobilized AuNP/PEDOT-MoS_2 based sensor electrode towards detection of goat-antimouse *IgG* was monitored through differential pulse voltammetry (DPV) technique in 0.1 M PBS solution containing 5 mM K_3 [Fe $(CN)_6$] as redox agent. Here, in Figure 3.8(a), the black curve represents the DPV response of the BSA/Antibody/Glu/AuNP/PEDOT-MoS_2 bioelectrode in absence of the antigen in the buffer solution. In the anodic scan of the DPV response, the broad peak appears around -0.1 V to 0.0 V potential range which also corresponds to the location of oxidation peak appearing in the CV response of mouse *IgG* immobilized AuNP/PEDOT-MoS_2 system. In CV response, the waveform of the applied potential is linear. While in case of DPV, the waveform is the superposition of both linear and staircase like waveforms, which gives the advantage of less contribution of capacitive or non-faradic current in the data acquired through DPV. As compared to the oxidation peak of CV, the surfaces of the DPV peaks are appeared to be uneven in Figure 3.8(a). This may be due to the sluggish kinetics of the redox process occurring after antibody immobilization where the additional dielectric layer of biomolecule hinders the mass transport as well as interfacial electron transfer towards the electrode system, giving rise to some distortion in the faradic current response. Afterwards, when goat-antimouse *IgG* was added in the solution, it binds selectively with the immobilized mouse *IgG* resulting in a drop in the redox active sites of the immunosensor probe. Hence, a lower current in the DPV response is realized after each subsequent addition of antigen in the solution. As can be seen in Figure 3.8(a), a proportional drop in current in the DPV response is attained on varying the antigen concentration from 7.7 to 545 ng/mL. The change in current (ΔI) with corresponding addition of antigen concentration ([C]) is plotted in Figure 3.8(b). And a substantial fit (R^2= 0.997) is obtained when the experimental data points are fitted *via* using Langmuir isotherm relation given by: $I = \frac{I_0}{1+\frac{B}{[C]}}$; where, I_o is saturated current response and B represents the inverse of Langmuir adsorption coefficient (k). Moreover, the linear relation between $1/\Delta I$ and $1/[C]$ as depicted in Figure 3.8(c), suggests the occurrence of diffusion process that would typically follow Langmuir adsorption isotherm behaviour. From the fitted parameters of Figure 3.8(b), the value of saturated current response (I_o) and adsorption coefficient (k) of antigen over our fabricated biosensor can be estimated to be 511 µA and 27.5 L. g^{-1} respectively. Again, in the ΔI *vs [C]* plot of Figure 3.8(d), we obtained two linear

regions in the concentration ranges, 7.7-263 ng/mL and 263-545.7 ng/mL, having regression relations y = 0.9228 x+13.04, (R^2= 0.984) and y = 0.3165 x+137.76, (R^2 = 0.995) respectively.

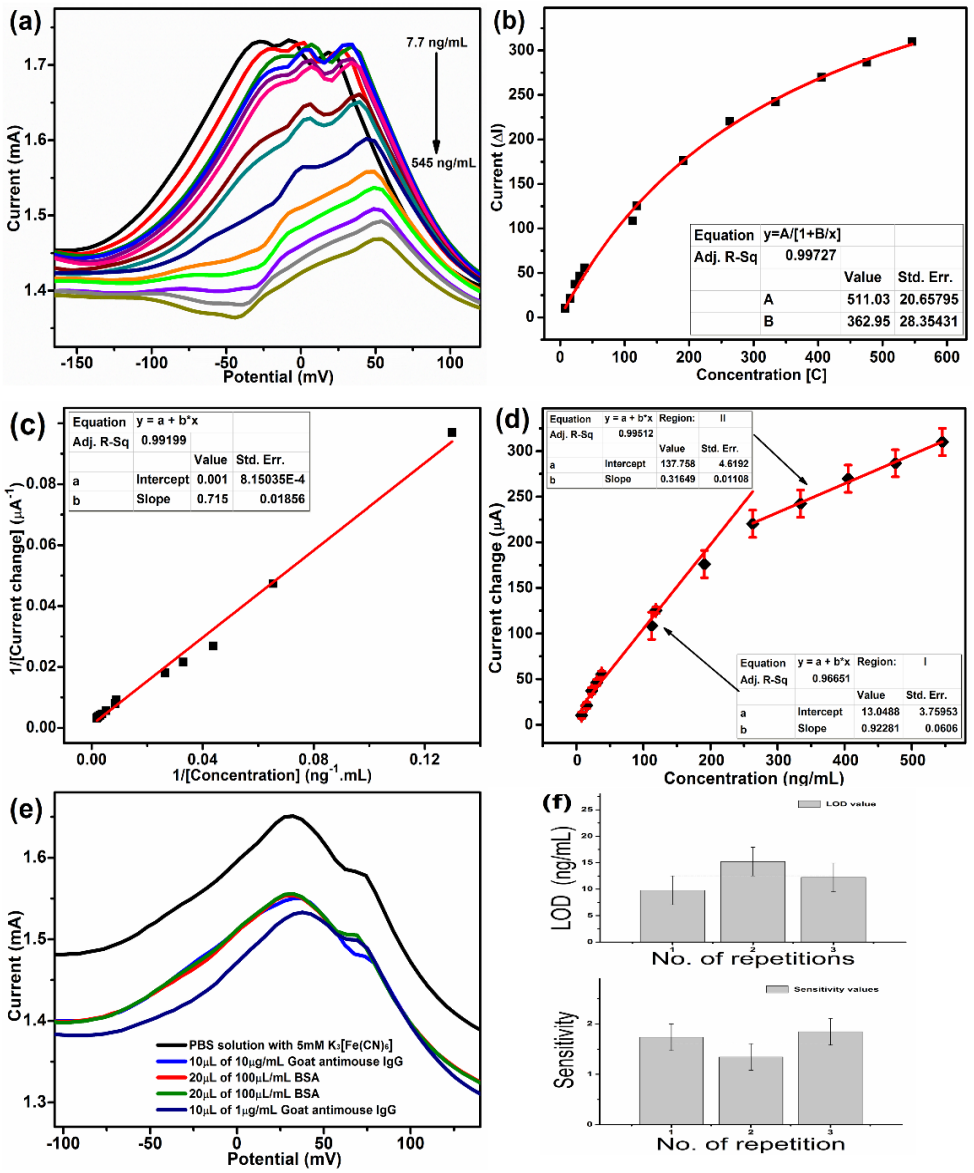

Figure 3.8: (a) DPV response of Antigen/BSA/Antibody/Glu/AuNP/ PEDOT-MoS_2 sensor upon addition of different concentration of antigen, (b) Langmuir fitting of ΔI *vs [C]* plot, (c) $1/\Delta I$ *vs* $1/[C]$ plot, (d) Linear fitting of ΔI *vs [C]* plot, (e) selectivity test for BSA/Antibody/Glu/AuNP/PEDOT-MoS_2 immunosensor, (f) comparison of *LOD* and selectivity estimated from three repetitive experiment

The *LOD* of our immunosensor towards detection of the specific antigen is estimated to be 12.22 ng/mL by using the formula $\frac{3.3\times\sigma_y}{m}$; where σ_y is the standard error of *y*-intercept and *m* is the slope of the linear regression line of Region-I. The sensor attains a sensitivity value of 1.8456 µA.ng^{-1} mL.cm^{-2} under a wide linear range of 7.7-263 ng/mL of specific antigen concentration. Furthermore, selectivity of our fabricated immunosensor towards the specific antigen was checked by monitoring the DPV current after addition of BSA in the electrolyte solution. BSA is an albumin protein extracted from cow serum usually used in immunoassay techniques. A biosensor is said to have good selectivity if it doesn't respond to another interfering biomolecule *eg.* BSA. In Figure 3.8 (e), one can view that the current in the DPV response changes appreciably upon addition of the target analyte (goat anti-mouse *IgG*). But the same DPV responses remained unchanged when 20 µL of 100 µL/mL BSA was added in the solution, denoted by red and green labelled curves. This shows that the immunosensor interact only with the target analyte in presence of other interfering molecules, illustrating the selectivity feature of our fabricated sensor.

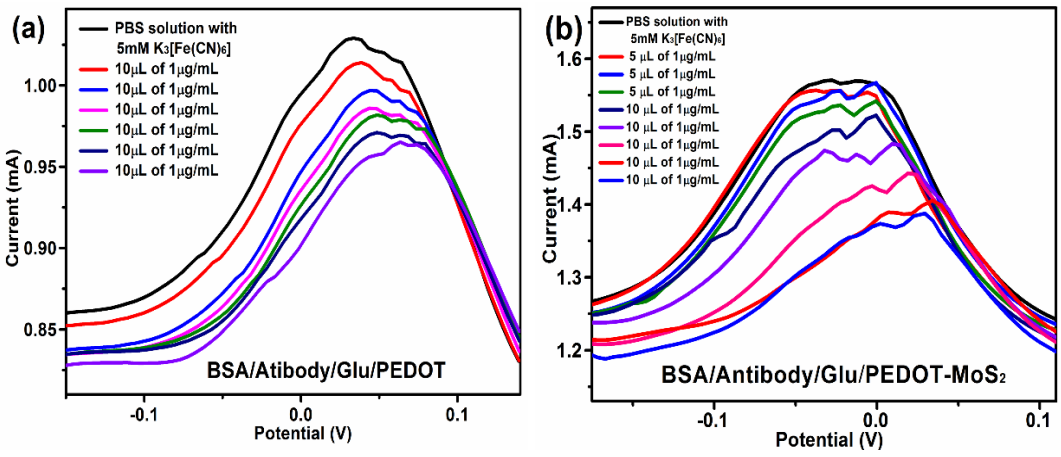

Figure 3.9: Detection of goat antimouse *IgG* using (a) BSA/Antibody/Glu/ PEDOT and (b) BSA/Antibody/Glu/PEDOT-MoS_2 bioelectrode by DPV technique performed in 0.1 M PBS solution containing 5 mM $K_3[Fe(CN)_6]$ as redox probe

Moreover, to compare the detection capability of the PEDOT and PEDOT-MoS_2 based sensors electrodes, the DPV responses were acquired for BSA/Antibody/Glu/PEDOT and BSA/Antibody/Glu/PEDOT-MoS_2 toward detection of the specific antigen, as shown in Figure 3.9 (a) and (b), respectively. In the PEDOT based immunosensor, diminution of current has been realized upon addition of 10 µL of 1 µg/mL (~15 ng/mL) antigen in the

650 µL of PBS solution (Figure 3.9 (a)). Whereas, in case of PEDOT-MoS_2 one, a distinct drop in the DPV current can be observed when 5 µL of 1 µg/mL (7.7 ng/mL) specific antigen is added in the solution. Noticeably, in both PEDOT and PEDOT-MoS_2 cases, the DPV current drop almost gets saturated after attaining a sum of ~100 ng/mL antigen concentration in the buffer solution. While in case of AuNP/PEDOT-MoS_2 system, a routine drop in current response was seen up to a higher concentration of added goat-anti-mouse *IgG* (~ 545 ng/mL) in the PBS solution as can be viewed in Figure 3.8(a); it would indicate a better performance of the AuNP/PEDOT-MoS_2 derived immunosensor probe. The repeatability of the AuNP/PEDOT-MoS_2 based immunosensor was examined by repeating the sensing experiment (Figure 3.10 (a), (b)) followed by comparing the sensing parameters which were estimated from the repetitive experiments. The overlapped error bars in Figure 3.8(f) indicate that the obtained values of *LOD* and sensitivity from the repetitive experiments do not deviate significantly from each other.

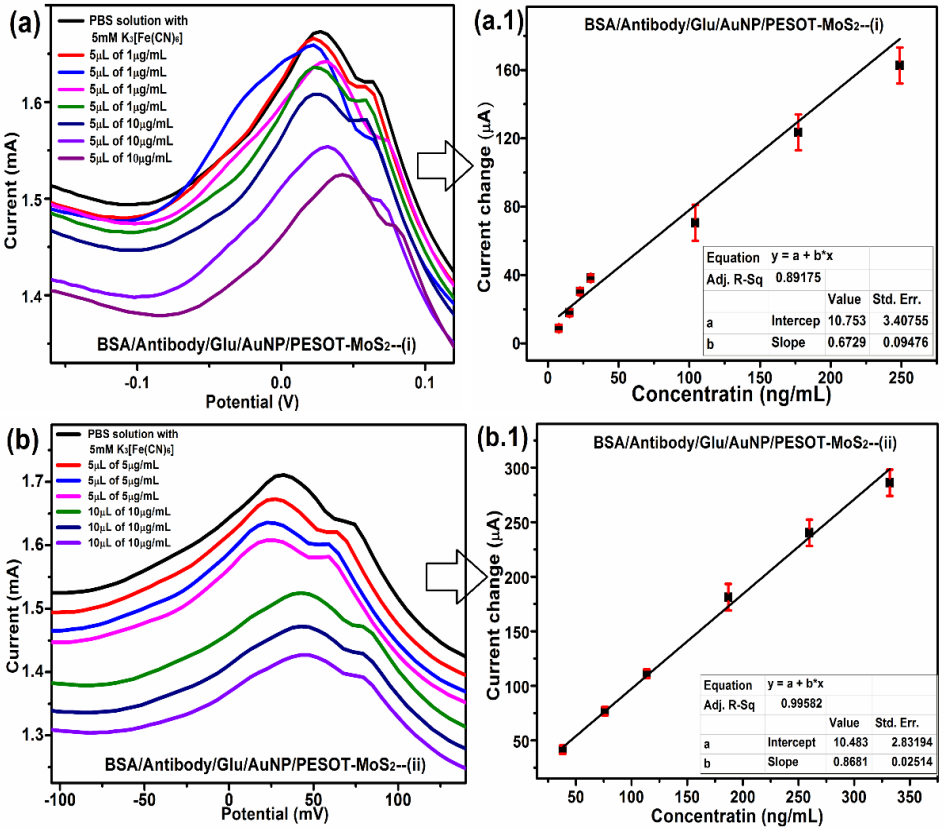

Figure 3.10: Repeatability test for BSA/Antibody/Glu/AuNP/PEDOT-MoS_2 bioelectrode (where the repeated experiments have been denoted as (i) and (ii))

3.4 Conclusions

An electrochemical immunosensor is fabricated in this work by immobilizing mouse *IgG* antibody over the electrochemically synthesized AuNP/PEDOT-MoS_2 hybrid nanosystem for detection of goat antimouse *IgG*. Structural, morphological and elemental analysis suggests the adequate incorporation of MoS_2 nanosheet in the polymer matrix followed by electrodeposition of AuNPs over the PEDOT-MoS_2 composite. A synergic enhancement in the electrochemical activity and interfacial charge transfer has been achieved after insertion of MoS_2 and surface anchoring of AuNPs in the polymer host. The physisorption of the antigen over the sensor electrode follows Langmuir isotherm offering a saturated current (I_o) value of 511 µA. The prepared biosensor exhibited a low *LOD* of 12.22 ng/mL and a sensitivity value of 1.8456 µA mL $ng^{-1}cm^{-2}$ within a wide linear range of 7.7-263 ng/mL for selective detection of specific antigen. Biosensors with a higher degree of sensitivity and selectivity have tremendous scope in diagnostics and in point of care (POC) remedial measures. This study has been executed mainly to overcome the drawbacks of the earlier work. A low *LOD* value with a moderate sensitivity response proposes the better performance of the studied immunosensor. Moreover, the comparison of the electrochemical parameters of the pristine and modified electrode systems have also helped in framing the contribution of each component in synergic enhancement of electrochemical performances. The major drawback of using such enzyme-based sensor is the short lifespan of the immunosensor as the bio-recognition elements are highly affected by the surrounding environment. So, development of enzyme free sensing protocol for detection of biological analytes can be an interesting avenue for further exploration.